

Semih Gürsu · M. Cemal Göncüoglu

## Petrogenesis and tectonic setting of Cadomian felsic igneous rocks, Sandıklı area of the western Taurides, Turkey

Received: 23 March 2005 / Accepted: 24 November 2005 / Published online: 20 January 2006  
© Springer-Verlag 2006

**Abstract** In the Sandıklı (Afyon) region, western Taurides, the Late Proterozoic rocks of the Sandıklı basement complex are composed of low-grade meta-sedimentary rocks (Güvercinoluk Formation) intruded by felsic rocks (Kestel Çayı Porphyroid Suite, KCPS). The KCPS is a deformed and highly sheared, dome-shaped rhyolitic body with a granitic core. Quartz porphyry dikes intrude both the slightly metamorphic igneous and the sedimentary rocks of the basement complex. Both the quartz porphyries and rhyolites were converted into mylonites with relict igneous textures. Geochemical data show that these felsic igneous rocks are subalkaline and mainly granitic in composition with  $\text{SiO}_2 > 72 \text{ wt\%}$  and  $\text{Al}_2\text{O}_3 > 11.5 \text{ wt\%}$ . The chondrite-normalized incompatible trace element patterns are characterized by distinct negative Rb, Nb, Sr, P, Ti, and Eu with enrichment in Th, U, La, Ce, Nd, Sm, and Zr. The REE patterns of the felsic rocks indicate a strong enrichment in LREE but display slightly flat HREE patterns. According to geochemical characteristics and petrogenetic modeling, extrusive and intrusive rocks of the KCPS were probably derived from an upper continental crustal source (partial melting of granites/felsic rocks) by 18–20% fractional melting plus 18–20% Rayleigh fractional crystallization, which seems to be the most effective igneous process during the crystallization of the KCPS. Single zircon age data from the granitoids and fossils from the disconformably overlying sedimentary successions indicate that the metamorphism and the igneous event in the Taurides are related to the Cadomian orogeny. Based on the geological, geochem-

ical and petrogenetic correlation of the post-collisional granitoids it is further suggested that the Tauride belt in western central Turkey was in a similar tectonic setting to the Gondwanan terranes in North Africa (Younger Granitoids) and southern Europe (Spain, France, Bohemia, Brno Massifs) during the Late Cadomian period.

**Keywords** I-type granites · Rhyolites/quartz porphyry rocks · Post-collisional · Taurides · Late Pan-African

### Introduction

Late Proterozoic granitic complexes with radiometric ages ranging from 550 to 530 Ma are important constituents in North Africa and in the Gondwana-derived terranes in Southern and Central Europe (Ballèvre et al. 2001; Chantraine et al. 2001; El-Nisr et al. 2001; Pin et al. 2002; Bandres et al. 2002; Dörr et al. 2002; Genna et al. 2002; Mushkin et al. 2003). These granitic complexes are known as the “Late Pan-African Granitoids” or “Cadomian Granitoids” and their formation was ascribed to a wide range of tectonic events to the north of the main part of Gondwana. The terms Cadomian and Pan-African are used here more or less synonymously, the former for tectonic elements in southern Europe that underwent orogenic overprint including granitoid magmatism and metamorphism in Late Neoproterozoic to Early Paleozoic times. The latter is used here for terranes still attached to Africa.

Based on the geochemical characteristics of these granitoids and the depositional features of the associated sediments these events have been related to different processes (Ballèvre et al. 2001; Chantraine et al. 2001; Bandres et al. 2002; Dörr et al. 2002; Genna et al. 2002). These events include:

- Southward subduction of the Iapetus ocean and formation of the continental arc-type magmatism;
- Granitic magmatism related to post-collisional extension;

S. Gürsu  
MAT Department, General Directorate of Mineral Research  
and Exploration, Ankara, Turkey  
E-mail: sgursu@yahoo.com

M. C. Göncüoglu (✉)  
Geological Engineering Department,  
METU, Ankara, Turkey  
E-mail: megoncu@metu.edu.tr  
Tel.: +90-312-2102681  
Fax: +90-312-2101263

- Back-arc basin development at the northern edge of Gondwana; and
- Collision-type magmatism related to the amalgamation of small Gondwana-derived continental microplates (peri-Gondwanan terranes).

In Anatolia, Precambrian rocks occur in the basement of different Alpine units in NW, S and SE Anatolia (Göncüoglu et al. 1997). The Tauride Belt in southern Turkey (Fig. 1) includes a basement complex with siliciclastic rocks, stromatolitic limestones, slates and felsic volcanic rocks, both in the eastern (e.g. Kozlu and Göncüoglu 1997) and western parts. A similar basement complex was also encountered in southeastern Turkey (Ketin 1966). These basement complexes were traditionally ascribed to the “Infracambrian” to include Eocambrian to Lower Cambrian rocks. A detailed account of the locations and rock units of this “Infracambrian” basement is given in Kozlu and Göncüoglu (1997).

Gürsu and Göncüoglu (2001) and Gürsu et al. (2004) recently described low-grade metamorphic sediments and felsic igneous rocks of the Late Proterozoic age in the Sandıklı area of the Taurides in western central Anatolia (Fig. 1). These authors have also shown that the Late Proterozoic basement rocks are overlain disconformably by siliciclastic rocks that contain Early Cambrian (Erdogan et al. 2004) trace fossils. Based on the single zircon ages of the granitic rocks in this area (Kröner and Sengör 1990) and the new stratigraphic findings (Gürsu and Göncüoglu 2001; Gürsu et al. 2004) these basement rocks were attributed to the Late Pan-African/Cadomian basement of Gondwana.

In this study, we will present geochemical data from the felsic igneous rocks within the Late Proterozoic basement of the Taurides in the western part of central Anatolia, and discuss their petrology, petrogenesis and tectonic setting to interpret their relationships to other Late Pan-African or Cadomian granitoids in northern Gondwanan terranes.

## Geological framework

In the western part of central Anatolia around Sandıklı (Fig. 1), the basement unit with low to very low-grade metamorphic rocks has been described by various authors (Öngür 1973; Kröner and Sengör 1990; Özgül et al. 1991; Kozlu and Göncüoglu 1995). Gürsu and Göncüoglu (2001) and Gürsu et al. (2004) pointed out that this unit actually includes the Sandıklı basement complex (SBC) and its Lower Paleozoic cover.

The SBC constitutes the meta-sedimentary rocks of the Güvercinoluk Formation and the felsic igneous rocks of the Kestel Cayı Porphyroid Suite (KCPS). The Güvercinoluk Formation consists of a very thick succession of dark colored phyllitic slates and/or phyllites with bands and lenses of black cherts, cherty dolomites, dark gray meta-sandstones and debris flow conglomer-

ates (Fig. 2). The siliciclastic meta-sediments show a relatively well-developed foliation and are characterized by the metamorphic paragenesis: quartz + albite + biotite + muscovite + graphite ± chlorite. The meta-sandstones include flattened clasts of basic volcanic rocks and black chert. The black cherts, interlayered with siliciclastic rocks, are 10–50 cm thick, finely laminated and very similar to the phthanites described in the Late Proterozoic sediments in NW Gondwanaland (Le Corre 1977; Chantraine et al. 1988, 2001; Bandres et al. 2002). The meta-carbonates within this formation form bands and lenses of light gray dolomites with very thin bands of cherts. Locally, they display stromatolithic textures.

Petrographical data on the Güvercinoluk Formation revealed that the phyllites, phyllitic slates with crenulation folds and mylonites mainly contain quartz, sericite, biotite, chlorite, feldspar and show textural evidence for three distinct deformational phases. Fine-grained biotite neoformations are typical and phyllosilicate paragenesis is characterized by illite/mica + mixed-layer chlorite-vermiculite (C-V) + chlorite-smectite (C-S) ± chlorite. The crystallinity values ( $\Delta^{\circ}2\theta = 0.14\text{--}0.24$ , mean = 0.20) of phengitic illite/muscovites of 2M<sub>1</sub> polytype are indicative of epimetamorphism, whereas the  $b_0$  values (9.028–9.058 Å, mean = 9.043 Å) suggest the higher parts of an intermediate- to high-pressure facies condition (Bozkaya et al. 2004).

The meta-sedimentary rocks of the Güvercinoluk Formation interfinger with highly deformed felsic pyroclastic rocks interpreted as rhyolitic crystal- and lithic-tuffs (Gürsu 2002) and are intruded by sills and dikes of meta-quartz porphyry (Fig. 2).

The KCPS comprises meta-rhyolites and irregularly distributed sills/dikes of meta-quartz porphyry. They occur in the core of the NNE–SSW trending antiform and have a core of mylonitic granitoids around the Büyükbakırlı and Kocayayla Hills (Fig. 1). Both the meta-rhyolites and their coarse grained equivalents are intensively mylonitized and variably foliated. The meta-rhyolitic rocks of the KCPS show illite/mica ± C-V phyllosilicate paragenesis, and display IC and  $b_0$  values similar to the Güvercinoluk Formation (Bozkaya et al. 2004).

Kröner and Sengör (1990) stated that the single zircon  $^{207}\text{Pb}/^{206}\text{Pb}$  ages obtained from the quartz porphyries vary between  $543 \pm 7$  and  $2,448 \pm 3$  Ma. The youngest age ( $543 \pm 7$  Ma) is interpreted to represent the time of granite intrusion, whereas the older ones reflect the age of the crustal source from which the granite may have been derived or through which the granite magma ascended.

The metaclastic rocks of the Gögebakan Formation cover the SBC (Fig. 2) by an angular unconformity. Discontinuous pockets of basal conglomerates with well-rounded pebbles derived from the felsic rocks, meta-carbonates and black cherts of the SBC are present in the lower part of the formation. The middle part of this formation comprises variegated arkoses,

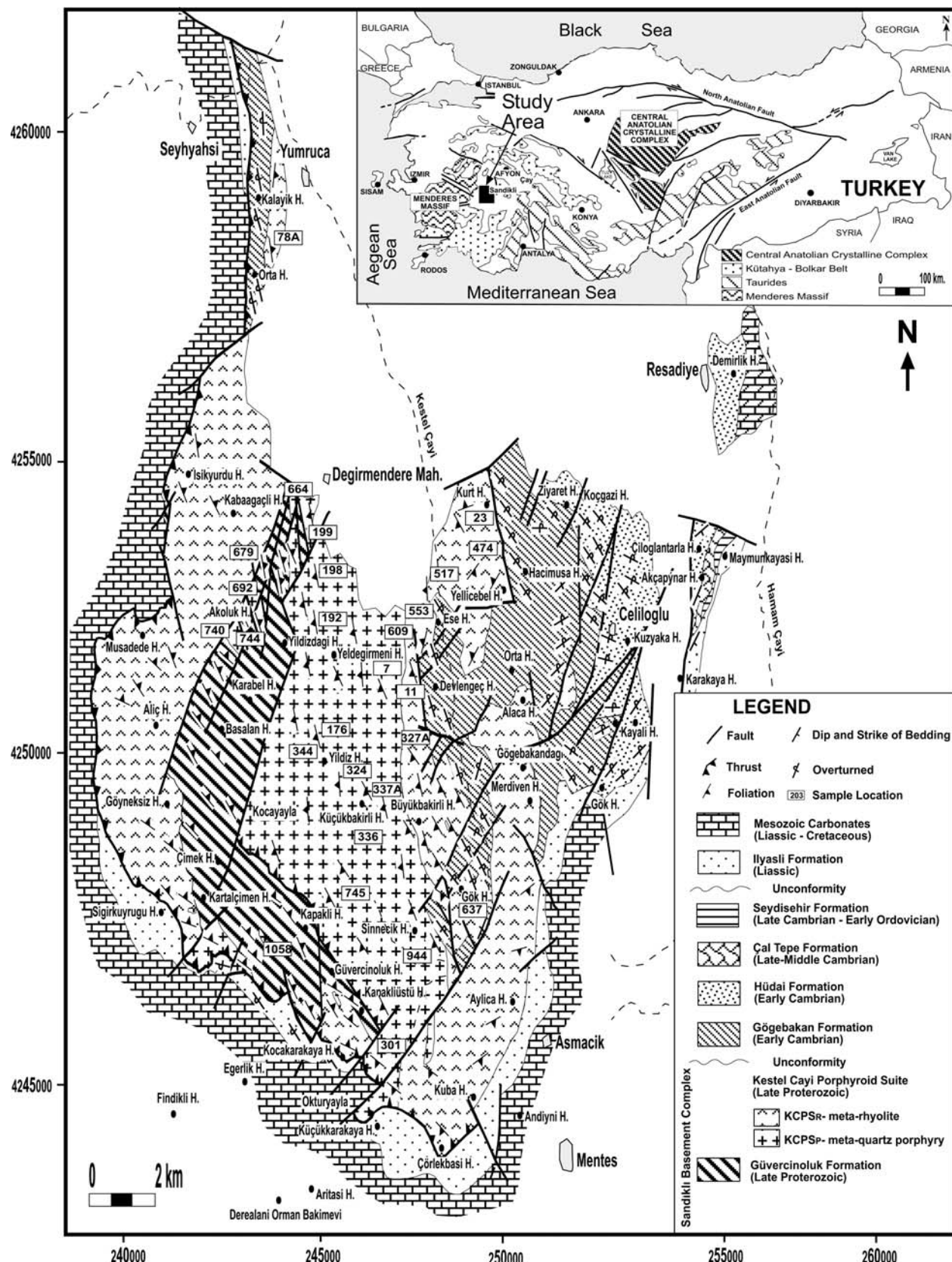


**Fig. 1** Geological map of the Sandikli area (Gürsu 2002). The inset map shows the location of the study area and the main tectonic units of the Tauride-Anatolide Belt (simplified after Göncüoglu et al. 1997)

meta-siltstones, black and green meta-mudstones. This succession includes spilitic lava-flows and lenses of dark green pyroclastic rocks and grade upwards into siliciclastic rocks of the Celiloglu Member of the Hüdai Formation (Fig. 2). This member is almost 100 m thick and is made up of an alternation of pink, white and yellow siliceous mudstones, quartz-siltstones and quartzites and continues upward into the thick-bedded quartzite of the Örenkaya Quartzite Member of Hüdai Formation. Based on trace fossils (Erdogan et al. 2004) at the transitional layers between the Celiloglu Member

and the Gögebakan Formation, a Tommotian (earliest Cambrian) age has been assigned to this unit.

The mudstones of the Gögebakan Formation typically display crenulation folds and only two foliations. Its metamorphic paragenesis is illite + chlorite  $\pm$  C-V  $\pm$  C-S. The illites/muscovites are of muscovitic-phengitic composition and 2M<sub>1</sub>-type, whereas the neo-formed ripidolitic chlorites are of the IIb polytype. The IC values ( $\Delta^2\theta = 0.14\text{--}0.27$ , mean = 0.20) are similar to those of the Güvercinoluk Formation but the  $b_0$  values (9.004–9.040 Å, mean = 9.026 Å) are lower and characterize an intermediate-pressure facies condition (Bozkaya et al. 2004).

Age	Formation	Lithology	Explanation
Liassic-Cretaceous	Mesozoic Carbonates	Limestone, Limestone-siltstone alternations	
Liassic	Ilyasli Formation	Conglomerate, sandstone, siltstone	
Late Cambrian-Early Ordovician	Seydisehir Formation	UNCONFORMITY Green-grey shale, siltstone Nodular limestone	
Late-Middle Cambrian	Cal Tepe Formation	Nodular limestone Dolomite, dolomitic limestone	
Early Cambrian	Orenkaya Quartzite Member	White, pink, reddish thick-bedded quartzite	
	Hüdai Formation	Quartz siltstone-shale-quartzite alternation Trace fossils	
Early Cambrian	Gögebakan Formation	Dark grey, violet, reddish meta-mudstone; arkosic meta-sandstone; meta-tuff with basic lava flows; meta-diabase dikes and sills Conglomerate with meta-rhyolite pebbles	UNCONFORMITY
Late Proterozoic	Kestel Cayi Porphyroid Suite	Meta-quartz porphyry Meta-rhyolite	
	Güvercinoluk Formation	Meta-siltstone, meta-sandstone with lydite, conglomerate and cherty limestone alternations	not scaled

Fig. 2 Generalized columnar section of the Sandıklı area (after Gürsu and Göncüoglu 2001)

## Petrography

Meta-rhyolites of KCPS are mylonitic-blastomylonitic with porphyroclasts of quartz, K-feldspar and plagioclase. Where preserved, the skeletal quartz phenocrysts reflect strong undercooling effects (Fig. 3a) and are

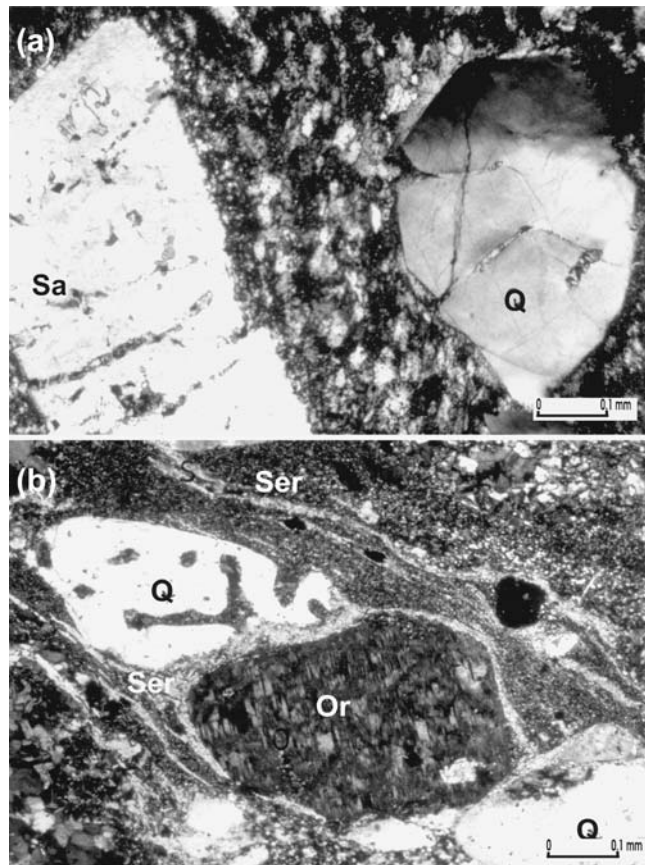


Fig. 3 a Microphotograph of the meta-rhyolites with the sanidine phenocrysts (Sa) displaying retrogression. The quartz porphyroclasts (Q) display typical skeletal structure and are surrounded by very fine-grained recrystallized quartz parallel to the mylonitic foliation. b Microphotograph of the meta-quartz porphyry rocks of the KCPS. The skeletal quartz (Q) and perthitic orthoclase (Or) porphyroclasts are surrounded by very fine-grained recrystallized quartz and neof ormations of sericite (Ser) parallel to the mylonitic foliation

euhedral to subhedral and deformed. In the mylonitic parts they are elongated and show a mortar texture. The phenocrysts of K-feldspar are strongly retrogressed and are obviously derived from twinned sanidine (Fig. 3a). The original plagioclase phenocrysts are replaced by albite subgrains (Gürsu 2002). The volcanic matrix preserved in larger porphyroclasts is mainly composed of quartz, K-feldspar (sanidine), plagioclase and white mica microcrysts. Accessory minerals are zircon and opaques. Epidote occurs as a secondary mineral. In general, the groundmass is replaced by neoformed/recrystallized quartz, albite and sericite (and coarse grained sericite-muscovite) as a product of extensive mylonitic deformation and very low-grade metamorphism.

The meta-quartz porphyries mainly include euhedral–subhedral quartz phenocrysts with a typical skeletal structure, euhedral–subhedral microperthitic orthoclase with micrographic texture and microcline phenocrysts (Fig. 3b). Mafic minerals are rarely preserved and occur as biotite relicts. Titanite, allanite, apatite, zircon and opaque minerals are the accessory phases (Gürsu 2002). In extremely deformed parts, the original minerals of the rock are only preserved as porphyroclasts. They are marginally recrystallized and surrounded by a mylonitic matrix with well-oriented and fine-grained metamorphic quartz and sericite neoformations.

## Geochemistry

### Analytical procedures

Twenty-seven representative samples (11 meta-rhyolites and 16 meta-quartz porphyry) were selected for major, trace and rare earth element (REE) analyses. Major, trace and REE element concentrations were determined in the ACME Analytical Laboratory (Canada/Vancouver) by using ICP-AES and ICP-MS. Representative major, trace and REE results are presented in Tables 1 and 2. Major elements ( $\text{SiO}_2$ ,  $\text{Al}_2\text{O}_3$ ,  $\text{Fe}_2\text{O}_3$ ,  $\text{CaO}$ ,  $\text{MgO}$ ,  $\text{Na}_2\text{O}$ ,  $\text{K}_2\text{O}$ ,  $\text{MnO}$ ,  $\text{TiO}_2$ ,  $\text{P}_2\text{O}_5$  and  $\text{Cr}_2\text{O}_3$ ) and the Ba and Sc trace elements were determined by ICP-AES after fusion with  $\text{LiBO}_2$ . The major elements detection limits are about 0.001–0.04% wt. The trace elements and REEs were determined by ICP-MS after acid decomposition ( $\text{HNO}_3$  of 5%). Detection limits of trace and REE elements are 10 ppm for Sc; 5 ppm for V; 2 ppm for Pb; 1 ppm for Ni, W, Sn and Zn; 0.5 for Ba, Co, Ga, Hf, Nb, Rb, Sr, Zr, La and Ce; 0.4 ppm for Nd; 0.1 for Cs, Ta, Th, Tl, U, Y and Sm; 0.05 for Eu, Gd, Dy, Ho, Er, Tm and Yb; 0.01 for Tb and Lu. Analytical precision, as calculated from replicate analyses, is 0.5% for the major elements and varies from 0.5 to 1.5% for trace and REEs.

### Major elements

The meta-rhyolites and meta-quartz porphyry rocks of KCPS yield similar compositions (see Tables 1, 2). As

they show evidence of dynamic metamorphism and mobility of the alkali elements (Gürsu 2002), geochemical diagrams used for discriminations were mainly based on the less-mobile elements (e.g. Winchester and Floyd 1977). On the  $\text{Zr}/\text{TiO}_2$  versus  $\text{SiO}_2$  diagram of Winchester and Floyd (1977) the meta-rhyolites and meta-quartz porphyry rocks are mainly rhyolitic in composition (Fig. 4) and plot in the subalkaline field.

Major and trace element distributions are illustrated on Harker variation diagrams (Fig. 5) where  $\text{Al}_2\text{O}_3$ ,  $\text{Fe}_2\text{O}_3$  and  $\text{TiO}_2$  decrease with increasing  $\text{SiO}_2$  and display negative trends (Fig. 5) compatible with the magmatic differentiation.  $\text{Na}_2\text{O}$ ,  $\text{K}_2\text{O}$  and  $\text{CaO}$  display poor negative correlation with increasing  $\text{SiO}_2$ . On the other hand,  $\text{P}_2\text{O}_5$  values of the meta-rhyolites display more linear trends than meta-quartz porphyry rocks with increasing  $\text{SiO}_2$ . The  $\text{MgO}-\text{SiO}_2$  variation diagram indicates a lack of linear relationship because of element mobility during the dynamic metamorphism (Fig. 5).  $\text{Al}_2\text{O}_3$ ,  $\text{Fe}_2\text{O}_3$ ,  $\text{TiO}_2$ ,  $\text{Na}_2\text{O}$ ,  $\text{CaO}$ ,  $\text{K}_2\text{O}$  and  $\text{P}_2\text{O}_5$  negative trends are broadly consistent with the fractionation of an assemblage consisting of plagioclase, alkali feldspar and iron oxides. Major element variations in meta-rhyolites and meta-quartz porphyry rocks are similar. The  $\text{Al}_2\text{O}_3/\text{TiO}_2$  versus  $\text{TiO}_2$  diagram represents a negative trend indicating the role of magmatic differentiation (Fig. 6).

Major elements with relatively poor correlation (e.g.  $\text{Na}_2\text{O}$ ,  $\text{CaO}$  and  $\text{MgO}$ ) were not used in further geochemical diagrams as this may be a result of element mobility during dynamic metamorphism.

### Trace and rare earth elements

The trace element versus  $\text{SiO}_2$  patterns are similar to the major elements (Fig. 5).  $\text{Sr}$  (8.3–39.5 ppm in meta-rhyolites, 16.5–63.9 ppm in meta-quartz porphyry rocks) and  $\text{Rb}$  (152.5–302.8 ppm in meta-rhyolites, 148–293 ppm in meta-quartz porphyry rocks) values decrease slightly with increasing  $\text{SiO}_2$  and are in accordance with the fractionation of an assemblage that includes alkali feldspar, plagioclase and biotite. The high value of Ba (757–1,545 ppm in meta-rhyolites, 496–1,623 ppm) displays no clear trend with increasing  $\text{SiO}_2$ , which may be due to dynamic metamorphism. The felsic rocks of the KCPS show a large scatter of data for V (5–29 ppm in meta-rhyolites, 5–33 ppm in meta-quartz porphyry rocks) and Zr (119–324.7 ppm in meta-rhyolites, 110.1–311.9 ppm in meta-quartz porphyry rocks) and sharp negative trends of V and Zr with increasing  $\text{SiO}_2$ , which were ascribed to the crystallization of biotite, Fe–Ti oxides and zircon. The negative correlation between Zr and  $\text{SiO}_2$  shows that the felsic melts were saturated in Zr and suggests that zircon was a fractionating phase. Zircon is microscopically observed in meta-rhyolites and meta-quartz porphyry rocks. On the other hand, Nb (10.1–22.8 ppm in meta-rhyolites, 9.4–17.9 ppm in meta-quartz porphyry rocks) decreases slightly with

**Table 1** Representative chemical analyses of the meta-rhyolites of KCPS

Sample No	11	23	78A	324	327A	474	517	553	609	637	679	Average
SiO <sub>2</sub>	72.94	77.03	75.4	73.36	74.91	76.48	76.78	74.42	76.19	75.83	77.75	75.55
Al <sub>2</sub> O <sub>3</sub>	13.06	11.5	12.03	13.34	11.44	12.11	11.27	12.23	12.44	12.46	11.73	12.14
Fe <sub>2</sub> O <sub>3</sub>	3.4	1.55	1.91	2.76	2.19	1.25	1.38	3.4	1.24	1.41	1.65	2.01
MgO	0.46	0.31	0.5	0.67	0.21	0.39	0.09	0.28	0.32	0.25	0.99	0.4
CaO	0.14	0.02	0.04	0.09	0.02	0.02	0.01	0.15	0.01	0.02	0.03	0.05
Na <sub>2</sub> O	2.38	0.07	0.11	2.1	0.13	0.1	0.13	1.55	0.12	0.16	0.24	0.64
K <sub>2</sub> O	5.95	7.89	8.42	7.94	10.06	8.43	9.43	7.16	9.22	8.21	5.27	7.99
TiO <sub>2</sub>	0.44	0.12	0.19	0.35	0.19	0.11	0.11	0.49	0.12	0.13	0.18	0.22
P <sub>2</sub> O <sub>5</sub>	0.08	0.01	0.02	0.07	0.03	<0.01	0.02	0.1	<0.01	<0.01	0.02	0.03
MnO	<0.01	<0.01	<0.01	<0.01	<0.01	0.02	<0.01	0.01	<0.01	<0.01	0.01	0.01
Cr <sub>2</sub> O <sub>3</sub>	0.024	0.02	0.026	0.015	0.018	0.008	0.05	0.057	0.01	0.002	<0.001	0.021
LOI	1.00	1.00	1.9	1.00	2.5	1.6	1.00	0.9	1.00	1.4	1.8	1.37
Total	99.99	99.64	100.66	101.86	101.84	100.62	100.46	100.93	100.78	100	99.85	100.6
Ba	906	813	876	1,346	1,144	757	1,436	1,472	768	1,017	1,545	1,088.18
Sc	9	5	15	7	6	6	4	9	5	6	5	7
Co	5.1	3	3.3	4.1	4.5	3.2	5.4	7.9	3	3.4	2.7	4.14
Pb	<3	<3	<3	<3	<3	<3	<3	<3	<3	<3	4	3
Zn	1	1	5	3	1	3	1	2	1	<1	7	2.36
Ni	50	121	93	45	61	54	147	134	84	74	52	83.18
Cs	1.9	2.1	5.4	3.4	2.4	1.8	2	1.8	2.4	2.5	3.2	2.62
Ga	18.5	12.5	21.2	23.4	13.2	20.6	8.6	13.4	20.3	21.5	17.2	17.31
Hf	8.5	4.9	7.6	10.2	6.8	5.5	5.2	8.3	4.5	5.3	5.9	6.6
Nb	14.9	10.1	2.8	18.5	12.2	13.5	12.2	16.2	14.3	12.8	12.6	12.9
Rb	258.7	240	251.5	269	289.7	262.7	257.9	235.9	302.8	299.5	152.5	256.38
Sn	7	5	7	5	7	7	6	6	9	8	5	6.54
Sr	39.5	18.5	35.5	33.1	24.8	10.2	21.7	29.9	8.3	10.8	26.4	23.52
Ta	1.1	1.1	1.6	1.3	1.2	1.2	1.2	2.3	1.8	1.7	1.4	1.44
Th	21.5	24.3	26.2	32.1	21.2	29	25.5	22	34.3	29.8	23.6	26.31
Tl	0.9	0.5	0.6	0.5	0.5	0.5	0.4	0.6	0.7	0.4	0.55	
U	5.5	3.3	5.2	4.3	3.9	5.1	3.2	4.1	5.7	4.6	5	4.53
V	29	<5	<5	16	9	5	<5	27	11	8	7	11.54
W	3	3	4	3	4	3	3	6	3	4	2	3.45
Zr	287.8	119	212.3	324.7	177.8	133.9	127.1	269.7	119.1	130.7	169	188.28
Y	47.6	40	87.7	40.6	51.1	38.1	44	39.8	62.9	49.1	40.8	49.24
La	42.6	41	63.2	69.3	94.9	81.2	86.7	42	41.3	15.9	47	56.82
Ce	86.6	90	135.2	140.4	196.9	172.7	162.3	89.5	94.1	27.1	97	117.41
Pr	9.86	9.91	15.22	15.42	21.45	19.38	17.37	10.41	10.23	3.91	10.54	13.06
Nd	35.5	35.1	58.5	54.8	75.7	68.2	60.8	42	37.8	15.6	41	47.72
Sm	7.6	6.5	12.8	10.3	15.7	13	12.8	8.1	7.3	3.4	7.7	9.56
Eu	0.7	0.12	1.14	0.83	0.99	0.3	0.54	0.56	0.1	<0.05	0.52	0.53
Gd	7.31	4.87	13.16	8.11	11.79	8.27	9.5	7.28	7.67	4.06	6.48	8.04
Tb	1.23	0.92	2.44	1.24	1.68	1.2	1.38	1.05	1.44	1.02	1.12	1.33
Dy	8	6.72	15.24	7.35	8.83	7.18	7.52	7.03	10.78	8.66	7.68	8.63
Ho	1.61	1.42	3.14	1.4	1.64	1.45	1.46	1.52	2.44	2.01	1.66	1.79
Er	5.03	4.69	9.36	4.34	4.91	4.4	4.5	4.53	7.09	6.01	4.84	5.43
Tm	0.69	0.66	1.23	0.58	0.66	0.63	0.63	0.63	1	0.85	0.63	0.74
Yb	4.54	4.41	8.49	4.18	4.67	4.37	4.1	4.36	7.14	6.06	4.64	5.18
Lu	0.69	0.67	1.19	0.68	0.72	0.66	0.62	0.64	1	0.85	0.68	0.76
Ti	2,637.8	719.4	1,139.05	2,098.25	1,139.05	659.45	659.45	2,937.55	719.4	779.35	1,079.1	1,264.4
Zr/Y	6.05	2.98	2.42	8.00	3.48	3.51	2.89	6.78	1.89	2.66	4.14	4.07
Th/Nb	1.44	2.41	9.36	1.74	1.74	2.15	2.09	1.36	2.40	2.33	1.87	2.62
Th/Y	0.45	0.61	0.30	0.79	0.41	0.76	0.58	0.55	0.55	0.61	0.58	0.562
Y/Nb	3.19	3.96	31.32	2.19	4.19	2.82	3.61	2.46	4.40	3.84	3.24	5.93
La/Nb	2.86	4.06	22.57	3.75	7.78	6.01	7.11	2.59	2.89	1.24	3.73	5.87
Ti/Y	55.42	17.99	12.99	51.68	22.29	17.31	14.99	73.81	11.44	15.87	26.45	29.11
(La/Yb) <sub>N</sub> <sup>a</sup>	6.34	6.28	5.03	11.2	13.73	12.56	14.29	6.51	3.91	1.77	6.84	8.04
(La/Sm) <sub>N</sub> <sup>a</sup>	3.53	3.97	3.11	4.23	3.8	3.93	4.26	3.26	3.56	2.94	3.84	3.67
(Gd/Yb) <sub>N</sub> <sup>a</sup>	1.3	0.89	1.26	1.57	2.05	1.53	1.88	1.35	0.87	0.54	1.13	1.31
Eu/Eu <sup>a</sup>	0.28	0.065	0.268	0.277	0.222	0.088	0.149	0.223	0.0408	–	0.225	0.167

<sup>a</sup>Normalization data from Sun and McDonough (1989)

increasing SiO<sub>2</sub>, while Y (38.1–78.7 ppm in meta-rhyolites, 29–69.6 ppm in meta-quartz porphyry rocks) generally rises with increasing SiO<sub>2</sub>. They have similar Ti/Zr (4.92–10.88 ppm in meta-rhyolites, 6.91–10.22 ppm in meta-quartz porphyry) and Nb/Y (0.22–0.45 ppm in

meta-rhyolites, 0.200–0.46 ppm in meta-quartz porphyry) ratios.

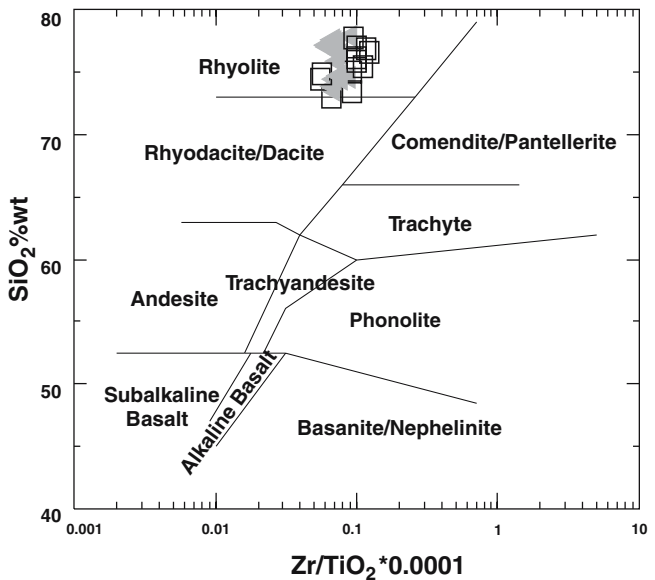
The average trace elements of meta-rhyolites and meta-quartz porphyry rocks are distinguished by having low Nb (12.9–14.48 ppm), Th (26.31–21.67 ppm)

**Table 2** Representative chemical analyses of the meta-quartz porphyry rocks of KCPS

Sample No	7	176	192	198	199	301	337A	336	344	664	692	740	744	745	944	945	1058	Average
SiO <sub>2</sub>	73.77	74.58	76.42	77.02	77.25	77.09	74.38	73.56	74.39	76.76	75.89	74.69	77.37	77.53	74.89	77.87	75.9	75.9
Al <sub>2</sub> O <sub>3</sub>	13.68	13.04	12.03	12.36	12.46	12.32	12.58	12.8	13.6	11.68	12.51	12.52	11.9	11.95	13.06	11.73	12.47	
Fe <sub>2</sub> O <sub>3</sub>	1.34	1.77	1.5	1.17	1.05	1.55	2.94	3.38	2.43	1.34	1.84	2.57	1.61	1.14	1.82	1.31	1.08	
MgO	0.51	0.68	0.77	0.39	0.67	0.5	0.27	0.26	0.49	0.21	0.45	0.66	0.47	0.43	1.1	0.37	0.51	
CaO	0.17	0.16	0.12	0.11	0.07	0.19	0.17	0.12	0.11	0.04	0.22	0.19	0.04	0.21	0.11	0.04	0.12	
Na <sub>2</sub> O	2.09	2.52	2.22	0.87	0.67	0.9	1.87	2.07	1.82	0.17	1.62	1.85	1.16	1.67	0.93	0.17	1.375	
K <sub>2</sub> O	6.31	5.25	4.73	5.43	6.67	5.61	6.09	5.93	4.81	7.79	5.26	5.11	5.73	5	6.12	7.81	5.32	
TiO <sub>2</sub>	0.48	0.3	0.16	0.19	0.17	0.29	0.4	0.39	0.36	0.14	0.27	0.28	0.2	0.17	0.37	0.14	0.26	
P <sub>2</sub> O <sub>5</sub>	0.08	0.06	0.02	0.05	0.05	0.05	0.08	0.05	0.05	0.08	0.11	0.08	0.1	0.05	<0.01	<0.01	0.07	
MnO	<0.01	<0.01	0.01	<0.01	<0.01	<0.01	<0.01	<0.01	<0.01	<0.01	<0.01	<0.01	<0.01	<0.01	<0.01	<0.01	0.01	
Cr <sub>2</sub> O <sub>3</sub>	0.016	0.002	<0.001	<0.001	<0.001	<0.001	<0.001	<0.001	<0.001	<0.001	<0.001	<0.001	<0.001	<0.001	<0.001	<0.001	0.0015	
LOI	1.3	2.1	1.5	1.8	1.3	1.3	1.1	1.3	1.1	1.3	1.9	1	1.4	1.5	1.4	1.1	0.8	1.41
Total	99.85	100.59	99.55	99.49	100.47	100.02	100.01	100.07	100.01	99.4	99.76	99.57	100.24	99.38	100.45	100.37	99.94	
Ba	870	1,110	496	792	899	1,099	1,542	1,369	863	1,563	1,623	723	2,373	634	785	1,003	1,124	
Sc	10	7	3	13	13	13	9	9	8	12	13	14	12	12	7	10	10.43	
Co	5.6	2.2	2.4	0.5	1.8	2.2	3	2.5	2.5	1.8	1.7	2.8	1.7	2.6	4	2.43		
Pb	<3	<3	5	7	22	<3	<3	<3	7	<3	<3	4	<3	4	3	7	5.03	
Zn	2	7	6	2	79	1	1	1	2	3	1	2	4	4	4	1	2.39	
Ni	67	30	37	14	31	60	24	12	13	63	13	34	16	11	11	37	31	
Cs	3.7	1.4	1.8	2.1	1.9	1.4	1.8	2.4	1.8	1.3	2.3	1.3	1.2	9.8	1.1	3.2		
Ga	21.6	21.2	15.8	19.5	21.9	19.9	16.9	15	18.1	15.4	20.5	21	20.4	20	15.8	14.5	18.55	
Hf	9.2	7.5	4	4.2	4.5	5.5	7.9	7.8	7	3.9	6.3	6.9	4.7	4.2	6.1	4.5	5.81	
Nb	15.8	15.7	9.4	13.6	15	17.9	14.3	13.3	13.9	15.6	16.2	16.8	15.7	12.7	11.6	13.9	14.48	
Rb	293	156.3	162.6	229.7	249.9	182.3	231.1	208.5	188.8	237.4	155.4	181	164	148	226.6	161.4	196.59	
Sn	6	6	4	4	5	4	4	3	4	6	5	5	4	4	5	7	4.79	
Sr	44.1	57	24.9	25.1	22.3	31.1	41	34.5	22.9	130.9	63.9	30.3	50.5	33.8	18.2	16.5	41.4	
Ta	1.3	1.2	1.3	1.4	1.6	1.1	1.1	1.1	1.4	1.9	1.5	1.4	1.5	1.4	1.2	1.8	1.48	
Th	22.3	27.9	17.5	15.1	15.5	23.8	25.3	22.9	24.8	20.8	21.4	25.4	17.6	13.4	23.3	15	19.89	
Tl	0.4	0.2	0.3	0.4	0.3	0.4	0.5	0.4	0.6	0.8	0.7	0.8	0.3	0.4	0.4	0.4	0.47	
U	6.5	4	2.6	4.3	3.2	4.2	2.6	2.9	3.4	4	4.3	2.4	5.3	3.2	5.7	3.3	3.88	
V	33	18	<5	5	7	10	16	13	14	7	10	13	6	<5	17	6	11.29	
W	3	3	2	3	2	2	3	2	2	1	1	2	1	2	4	1	2.07	
Zr	311.9	248.3	116.9	113.8	116.4	170	292.9	250.4	236.5	97	189.8	199	130.8	110.1	209.4	121.3	178.7	
Y	47.8	51.9	46.9	48.2	43.1	62.6	38.8	29	36.4	37.2	57.7	69.6	52.5	42.3	44.1	47.5	47.54	
La	49.7	59.3	30.1	21.6	31.4	53.6	58.5	64	47.3	18.6	53	61.4	35.3	24.1	45.9	34.3	42.55	
Ce	102.4	109	57.6	48.5	68.5	107.9	115.9	128.9	99.8	40.4	114.1	130	76.5	53.9	92.1	72.5	87.95	
Pr	11.42	13.06	7.66	5.75	7.8	12.96	14.27	11.25	4.81	13.07	14.94	8.9	6.23	10.78	44.1	47.5		
Nd	41.7	46.4	29.1	22.6	31.6	51.7	55.5	42.8	19.5	52.3	57.8	34.7	23.6	43.2	34.2	34.2	39.63	
Sm	8.9	9	6.5	5.8	7.5	10.8	9	9.6	7.5	5.2	10.3	12.3	8	6.4	8.9	7.4	8.32	
Eu	0.81	0.65	0.33	0.37	0.42	0.87	0.71	0.94	0.66	0.29	0.72	0.94	0.19	0.32	0.71	0.44	0.58	
Gd	7.44	8.21	6.43	6.32	6.89	10.43	8.02	7.4	6.84	5.29	9.7	11.57	7.67	5.94	7.8	6.79	7.68	
Tb	1.23	1.46	1.2	1.23	1.18	1.7	1.23	0.98	1.01	1	1.58	1.88	1.41	1.17	1.19	1.22	1.3	
Dy	8.15	9.19	8.03	8.52	8.27	11.73	7.38	6.07	6.53	6.97	10.62	12.47	9.86	7.78	8.03	8.65	8.7	
Ho	1.6	1.73	1.78	1.81	2.5	1.57	1.15	1.47	1.52	2.33	2.88	2.06	1.66	1.73	1.87	1.87		
Er	4.96	5.24	5.09	5.39	5	7.32	4.12	3.29	3.97	4.2	6.64	7.79	5.86	4.83	4.72	5.5	5.01	
Tm	0.66	0.71	0.7	1.01	0.59	0.46	0.55	0.6	0.93	1.09	0.82	0.7	0.66	0.78	0.74	0.74	0.74	
Yb	4.92	4.46	4.78	5.54	4.88	6.89	4.1	3.14	3.86	4.34	6.49	7.69	5.82	4.87	4.28	5.58	5.15	
Lu	0.7	0.68	0.68	0.71	0.7	0.95	0.56	0.49	0.54	0.59	0.9	1.12	0.79	0.66	0.62	0.73	0.72	

**Table 2** (Contd.)

Sample No	7	176	192	198	199	301	337A	336	344	664	692	740	744	745	944	1058	Average
Ti	2,877.6	1,798.5	959.2	1,139.05	1,019.15	1,738.55	2,398	2,338.05	2,158.2	839.3	1,618.65	1,678.6	1,199	1,019.15	2,218.15	839.3	1,584.86
Zr/Y	6.53	4.78	2.49	2.36	2.70	2.72	7.55	8.63	6.50	2.61	3.29	2.86	2.49	2.60	4.75	2.55	3.97
Th/Nb	1.41	1.78	1.86	1.11	1.03	1.33	1.77	1.72	1.78	0.69	1.32	1.51	1.12	1.06	2.01	1.08	1.39
Th/Y	0.47	0.54	0.37	0.31	0.36	0.38	0.65	0.79	0.68	0.29	0.37	0.36	0.34	0.32	0.53	0.32	0.43
Y/Nb	3.03	3.31	4.99	3.54	2.87	3.50	2.71	2.18	2.62	2.38	3.56	4.14	3.34	3.33	3.80	3.42	3.31
La/Nb	3.15	3.78	3.20	1.59	2.09	2.99	4.09	4.81	3.40	1.19	3.27	3.65	2.25	1.90	3.96	2.47	2.95
Ti/Y	60.20	34.65	20.45	23.63	23.65	27.77	61.80	80.62	59.29	22.56	28.05	24.12	22.84	24.09	50.30	17.67	35.32
$(\text{La}/\text{Yb})_{\text{N}}^{\text{a}}$	6.83	8.98	4.26	2.63	4.35	5.26	9.64	13.77	8.28	2.9	5.52	5.4	4.1	3.34	7.25	4.15	5.88
$(\text{La}/\text{Sm})_{\text{N}}^{\text{a}}$	3.51	4.15	2.91	2.34	2.64	3.12	4.09	4.2	3.97	2.25	3.24	3.14	2.78	2.37	3.25	2.92	3.14
$(\text{Gd}/\text{Yb})_{\text{N}}^{\text{a}}$	1.23	1.49	1.09	0.92	1.14	1.23	1.59	1.91	1.44	0.99	1.21	1.22	1.07	0.99	1.48	0.99	1.24
$\text{Eu}/\text{Eu}^{\text{a}}$	0.304	0.231	0.155	0.187	0.178	0.250	0.255	0.34	0.282	0.169	0.22	0.24	0.074	0.159	0.26	0.189	0.21

<sup>a</sup>Normalization data taken from Sun and McDonough (1989)**Fig. 4** Classification of the felsic rocks of KCPS (after Winchester and Floyd 1977). Open squares meta-rhyolite, filled triangles meta-quartz porphyry

and V (11.54–11.29 ppm); low to moderate Y (49.24–47.54 ppm); moderate La (56.82–42.55 ppm) and Ce (117.41–87.95 ppm) values, respectively (Tables 1, 2).

The trace and REE element patterns of the studied rocks are relatively similar, especially for LREE and HREE (Fig. 7a, b). Chondrite-normalized (Sun and McDonough 1989) trace element spider diagrams reveal that both groups display a humped pattern with sharp negative anomalies for Rb, Nb, Sr, P and Ti with enrichment in Th, U, La, Ce, Nd, Sm and Zr. They have similarities with the upper continental crust than with the lower continental crust and OIB (Fig. 7a).

Felsic rocks as a whole are enriched (Fig. 7b) in LREE [in meta-rhyolites La = 154.8 × chondrite and La = 109.3 × primitive mantle; in meta-quartz porphyry rocks La = 116 × chondrite and La = 81.8 × primitive mantle; normalization values from Taylor and McLennan (1995)] and display a slightly horizontal trend by MREE and HREE (Lu = 19.9 × chondrite, Lu = 10.3 × primitive mantle in meta-rhyolites; Lu = 18.8 × chondrite, Lu = 9.7 × primitive mantle in meta-quartz porphyry rocks).

Considering the REE patterns, the meta-rhyolites and meta-quartz porphyry rocks are clearly enriched in LREE and have roughly flat, unfractionated HREE patterns, which are similar with the upper continental crust rather than the lower crust and OIB (Fig. 7b). Taylor and McLennan (1995)'s chondrite-normalized  $(\text{La}/\text{Yb})_{\text{N}}$ ,  $(\text{La}/\text{Sm})_{\text{N}}$  and  $(\text{Gd}/\text{Yb})_{\text{N}}$  ratios show a large scatter data in meta-rhyolites (1.77–14.29; 2.94–4.26; 0.54–2.05) and meta-quartz porphyry rocks (2.63–13.77; 2.25–4.20; 0.92–1.91) and resemble the upper continental crust (9.21; 4.20; 1.40) rather than the lower crust (3.38; 2.18; 1.15) and OIB (11.58; 2.33;

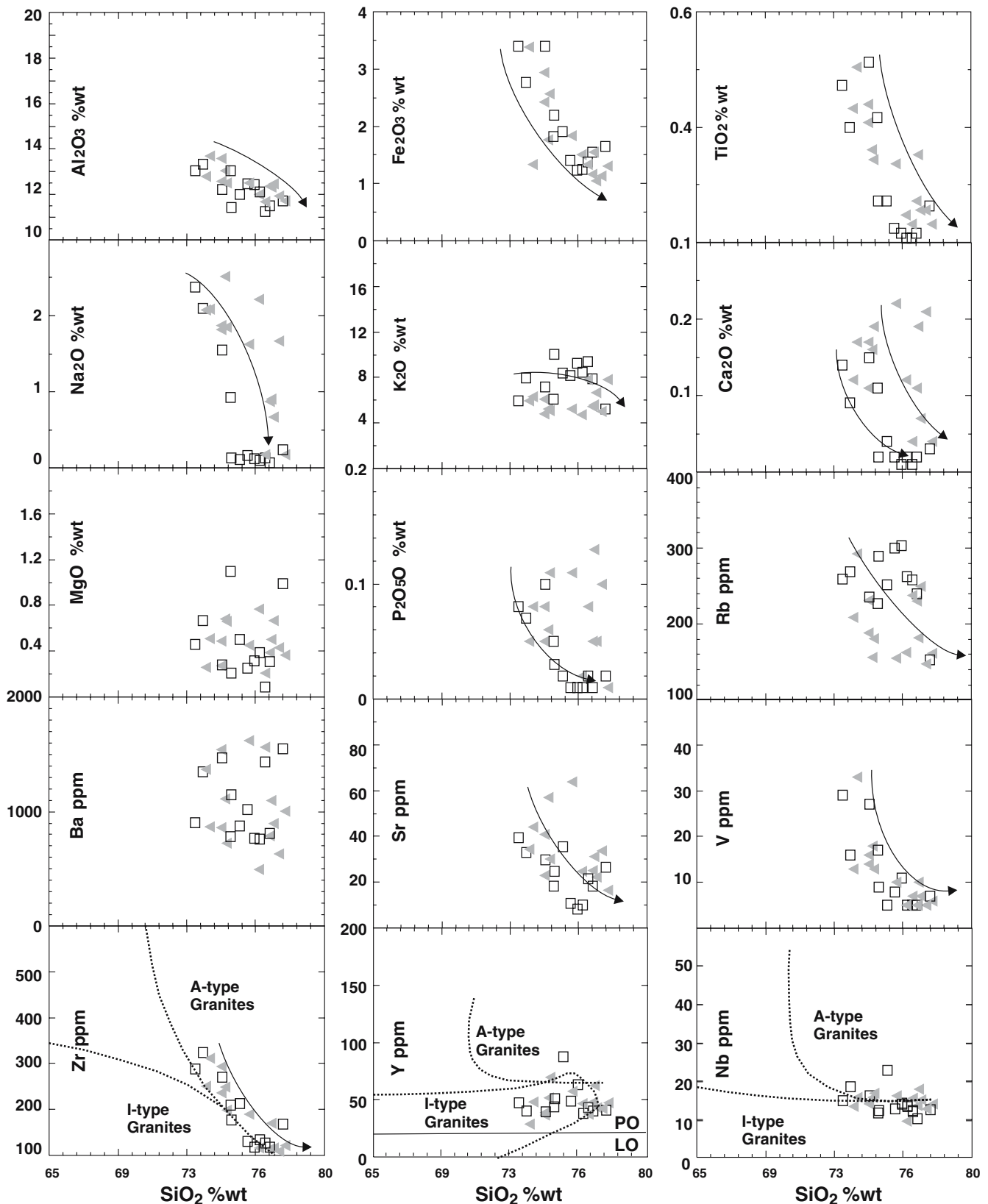


**Fig. 5** Harker diagrams illustrating the correlation of  $\text{Al}_2\text{O}_3$ ,  $\text{Fe}_2\text{O}_3$ ,  $\text{TiO}_2$ ,  $\text{Na}_2\text{O}$ ,  $\text{K}_2\text{O}$ ,  $\text{CaO}$ ,  $\text{MgO}$  and  $\text{P}_2\text{O}_5$  and  $\text{Rb}$ ,  $\text{Ba}$ ,  $\text{Sr}$ ,  $\text{V}$ ,  $\text{Zr}$ ,  $\text{Y}$  and  $\text{Nb}$  versus increasing  $\text{SiO}_2$ . Field boundaries for I- and A-type granites are from Collins et al. (1982). Symbols are the same as in Fig. 4

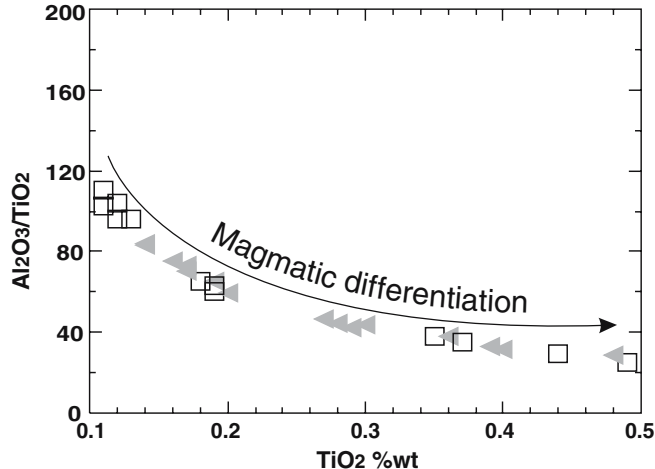


**Fig. 6** Distribution of the KCPS samples on the  $\text{Al}_2\text{O}_3/\text{TiO}_2$ – $\text{TiO}_2$  variation diagram. Symbols are the same as in Fig. 4

2.86). The patterns also display distinct negative Eu anomalies demonstrated by the  $\text{Eu}/\text{Eu}^*$  values of 0.07–0.28 for meta-rhyolites and of 0.16–0.33 for meta-quartz porphyry rocks (Fig. 7b). The presence of significant Eu and Sr negative anomalies are probably the result of early crystallization of feldspars from the melts by fractional crystallization or retention of these elements in feldspar at the source during the partial melting. The distinct negative Sr anomaly of the felsic rocks of KCPS may also be ascribed to mobilization during the dynamic metamorphism. The low to unfractionated HREE and Y patterns on the other hand suggest that the felsic magmas were produced outside the garnet stability field.

To summarize, geochemical variation diagrams confirm that the extrusive and intrusive felsic members of the KCPS are subalkaline in composition and belong to a co-genetic suite. The trace element patterns of the felsic rocks are very similar to each other with distinctive depletions in Nb, Sr, P and Ti relative to the other trace elements and enrichment in most incompatible elements (Th, U, La, Ce, Nd, Sm and Zr). Moreover, both the trace and REE patterns correlate very well with the upper crustal data.

### Source rock characteristics

Because of possible element mobility during the metamorphism of KCPS rocks, diagrams involving  $\text{CaO}$ ,  $\text{MgO}$ ,  $\text{Na}_2\text{O}$  and  $\text{K}_2\text{O}$  and the alumina saturation index (ASI) were avoided to reveal the source characteristics. The  $\text{Al}_2\text{O}_3$  versus  $\text{SiO}_2$  ratios were used to identify the compositional differences of computed melts produced by the partial melting of different source rocks (e.g. basaltic/amphibolitic rocks, undersaturated basaltic/amphibolitic, unsaturated/saturated basalts) (Helz 1976; Spulber and Rutherford 1983; Beard and Lofgren 1989, 1991; Winther and Newton 1991; Wolf and Wyllie

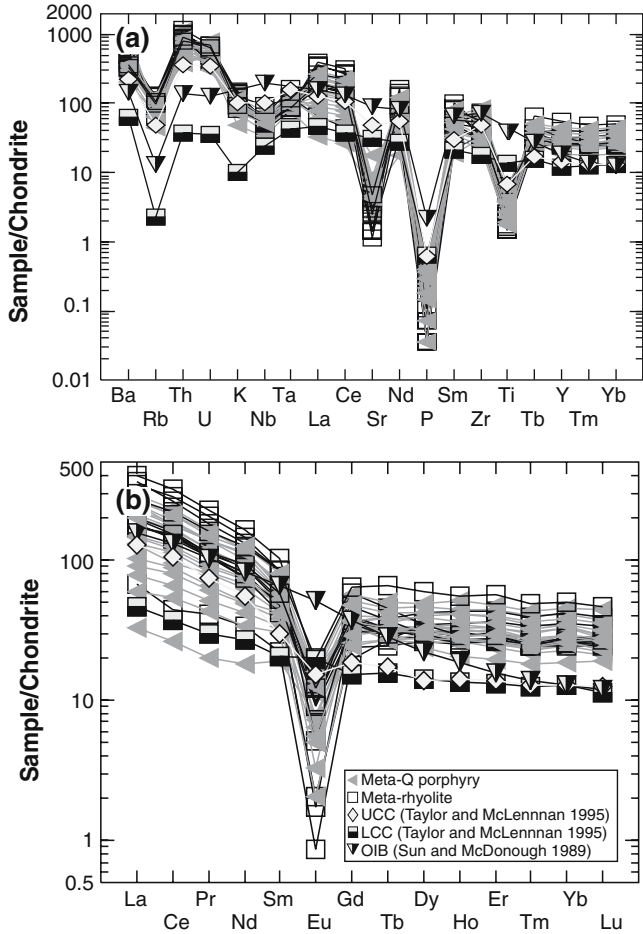
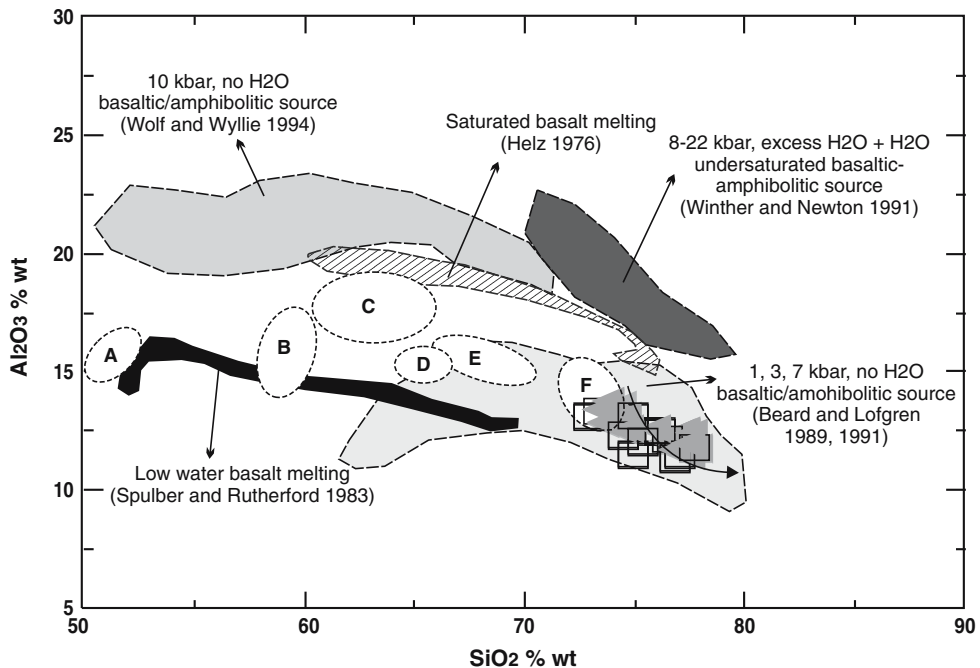


**Fig. 7** **a** Chondrite-normalized multivariation diagram (normalizing values from Sun and McDonough 1989). **b** Chondrite-normalized REE diagram (normalizing values from Sun and McDonough 1989). Open squares meta-rhyolites, filled triangles meta-quartz porphyry, half-closed squares upper continental crust data (Taylor and McLennan 1995), half-closed circle lower continental crust data (Taylor and McLennan 1995), filled diamond oceanic island basalt (OIB from Sun and McDonough 1989)

1994). The data of the Archean–Proterozoic–Phanerozoic andesites, basalts/komatites, cratonic shales, graywackes, granites and felsic rocks and tonalites-trondjemite-granodiorites (data taken from Condé 1993) are also plotted on the diagram to determine the protoliths of the KCPS. On the  $\text{Al}_2\text{O}_3$ – $\text{SiO}_2$  variation diagram (Fig. 8), the meta-rhyolites and meta-quartz porphyry rocks of KCPS plot towards the silica-rich end of basaltic/amphibolitic source field. The compositions of the meta-rhyolites and meta-quartz porphyry rocks overlap with the field for “low  $\text{H}_2\text{O}$  to dry” conditions, suggesting the 20–50% dehydration melting of a basaltic/amphibolitic source at 900–1,000°C and 1–7 kbar (Beard and Lofgren 1989, 1991). However, their magmatic protoliths are probably homogeneous and may be derived from high silica peraluminous Archean–Proterozoic–Phanerozoic granites/felsic rocks and from highly fractionated anatexic crustal melts and/or by the low and variable degrees of partial melting which resulted in

**Fig. 8**  $\text{SiO}_2$  versus  $\text{Al}_2\text{O}_3$  variations of felsic rocks of KCPS compared with the experimental result of the melting of meta-sedimentary, meta-pelite, unsaturated/saturated basalt and basaltic/amphibolitic sources and the data of the Archean–Proterozoic–Phanerozoic aged basalts/komatites (A), andesites (B), cratonic shales (C), graywackes (D), tonalities–trondjemite–granodiorites (E) and granites and felsic rocks (F) sources. The Archean–Proterozoic–Phanerozoic data are taken from Chondie (1993). Symbols are the same as in Fig. 4



a highly felsic composition. Meta-rhyolites/meta-quartz porphyry rocks may represent high silica felsic rocks of a low degree of partial melting and fractionation. The absence of the hydrated minerals such as amphibole and the very limited amount of biotite in the felsic rocks suggest that the partial melting of the protolith took place under “low  $\text{H}_2\text{O}$ ” conditions. Furthermore, the

$\text{Al}_2\text{O}_3/\text{TiO}_2$  versus  $\text{TiO}_2$  diagram also suggests that the extrusive and intrusive rocks may have been generated from a chemically similar magma source. The major and trace element characteristics, subalkaline character and the occurrence of titanite, rutile,  $\pm$  magnetite and  $\pm$  biotite as accessory minerals suggest that they both belong to the I-type granitoids (Chappell and White 1974).

**Table 3** Parameters used in the modeling of 18% fractional melting plus 18% Rayleigh fractional crystallization of the upper continental crust to produce the meta-rhyolite of KCPS and 20% fractional melting plus 20% Rayleigh fractional crystallization of the upper continental crust to produce meta-quartz porphyry rocks of KCPS

	$D_{0M}$	$C_{0M}$	18% Fractional Crystallization	Average of meta-rhyolites	$D_{0Q}$	$C_{0Q}$	20% Fractional Crystallization	Average of meta-quartz porphyries
Rb	0.95189	205.93	207.90	256.38	0.95725	198.66	200.56	196.59
Th	0.01954	21.36	25.94	26.31	0.09078	17.93	21.96	19.89
U	0.04263	3.67	4.43	4.53	0.0988	2.76	3.37	3.88
Nb	0.0048	9.12	11.11	12.9	0.45019	5.49	6.20	14.48
Sr	2.4030	49.52	37.48	23.52	2.3484	50.61	37.45	41.4
Zr	0.0267	191.03	231.73	188.28	0.12009	137.15	166.90	178.7
Ti	0.01882	3,285.92	3,992.28	1,324.35	0.0223	2,691.8	3,348.04	1,584.86
Y	0.0104	41.20	50.14	49.24	0.10971	39.63	48.34	47.54
La	0.07865	54.98	66.01	56.82	0.50556	53.06	59.25	42.55
Ce	0.04643	116.99	141.36	117.41	0.37275	112.8	129.74	87.95
Nd	0.04103	42.78	51.74	47.72	0.23534	41.72	49.48	39.63
Sm	0.03191	6.44	7.80	9.56	0.19279	6.34	7.59	8.32
Eu	2.8137	0.27	0.188	0.53	2.91606	0.27	0.18	0.58
Gd	0.01	8.59	10.45	8.04	0.0421	7.77	9.65	7.68
Tb	0.01988	0.84	1.02	1.33	0.15294	0.83	1.00	1.30
Dy	0.04396	7.56	9.14	8.63	0.16781	7.08	8.52	8.70
Er	0.0036	5.19	6.32	5.43	0.0326	4.67	5.79	5.01
Yb	0.02973	2.94	3.56	5.18	0.13726	2.90	3.51	5.15
Lu	0.03031	0.439	0.532	0.76	0.14785	0.43	0.52	0.72

$C_{0M}$  trace elements of the theoretical magma obtained from 18% fractional melting of the upper continental crustal source,  $C_{0Q}$  trace elements of the theoretical magma obtained from 20% fractional melting of the upper continental crustal source,  $D_{0M}$  the bulk partition coefficients of the modal composition of meta-rhyolites of KCPS,  $D_{0Q}$  the bulk partition coefficients of the modal composition of meta-quartz porphyry rocks of KCPS

This is also supported by the Nb–SiO<sub>2</sub>, Y–SiO<sub>2</sub> and Zr–SiO<sub>2</sub> diagrams (Fig. 5), where the studied samples mainly concentrate in the I-type granitoid field.

## Magma modeling

A trace element modeling was carried out for the identification of the source and magmatic processes. The upper continental crust composition of Taylor and McLennan (1995) was used as the possible source rock (Co) and the fractional melting and (Rayleigh) fractional crystallization processes were modeled by using Rb, Th, U, Nb, Sr, Zr, Ti, Y, La, Ce, Nd, Sm, Eu, Gd, Tb, Dy, Er, Yb and Lu. The normative composition of the upper continental crust (Taylor and McLennan 1995) assigned 16.1% quartz, 46.9% plagioclase, 20.1% orthoclase, 5.8% clinopyroxene, 10.0% orthopyroxene and 1% ilmenite. Quartz, plagioclase, orthoclase, clinopyroxene and orthopyroxene mineral/melt partition coefficients for rhyolitic melts were taken from Arth (1976), Pearce and Norrry (1979), Watson and Harrison (1983) and Nash and Crecraft (1985) (See Appendix).

Based on their average modal composition (Gürşar 2002), an assemblage of 39% quartz, 53% alkali feldspar

and 8% plagioclase in meta-rhyolites and of 35% quartz, 40% alkali feldspar, 18% plagioclase and 7% biotite in the meta-quartz porphyry rocks of KCPS were considered and calculated for the bulk partition coefficients (Do). For the modeling of fractional melting and Rayleigh crystallization, the formulas  $C_L/C_o = 1/D_o(1-F)^{(1/D_o-1)}$  and  $C_L/C_o = F^{(D-1)}$  (Rollinson 1993) were used for the meta-rhyolites and meta-quartz porphyry rocks of the KCPS, respectively. The computed trace element data for 1, 5, 10, 15, 18, 20, 25 and 30% fractional melting were determined and evaluated.

By 18 and 20% fractional melting, the computed magma composition had similarities with the average chemical analyses of the extrusive and intrusive rocks of KCPS. To achieve a better correlation, Rayleigh fractional crystallization of the theoretical magma by 18 and 20% were computed (Table 3). By 18% fractional crystallization of this theoretical magma and 20% partial melting plus 20% fractional crystallization, there is an optimal correlation on the chondrite-normalized (Sun and McDonough 1989) trace element spider diagrams with the meta-rhyolites and meta-quartz porphyry rocks, respectively.

Here, both groups display a clear parallel pattern with sharp negative anomalies in Rb, Nb, Sr and Ti with

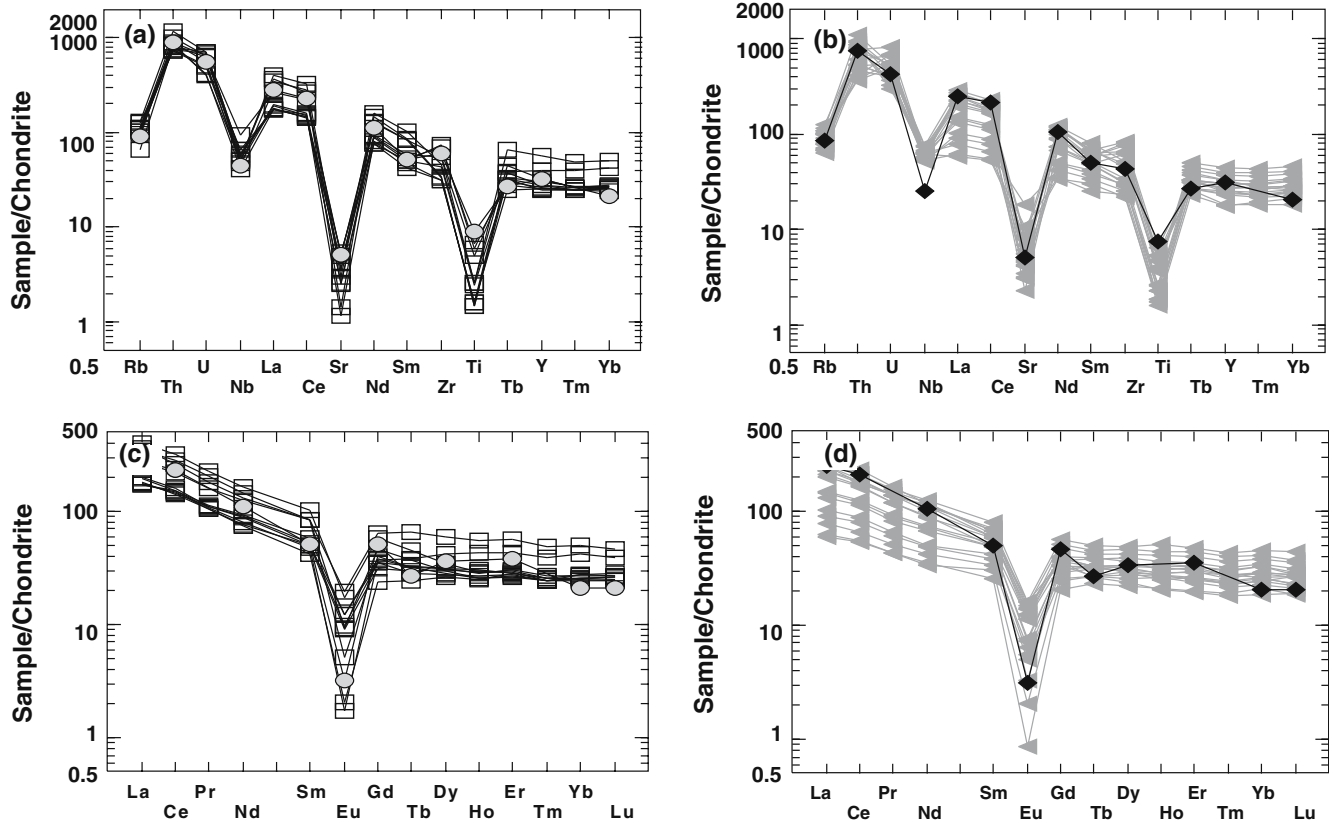


**Fig. 9** Multielement and REE spider diagrams for the meta-rhyolites and meta-quartz porphyry rocks and their comparison with the calculated composition for 18–20% fractional melting and 18–20% Rayleigh fractional crystallization. Open squares meta-rhyolite, filled triangles meta-quartz porphyry, closed circle meta-rhyolite obtained from 18% fractional melting plus 18% Rayleigh

fractional crystallization of the upper continental crust data of Taylor and McLennan (1995), closed diamond meta-quartz porphyry obtained from 20% fractional melting plus 20% Rayleigh fractional crystallization of the upper continental crust data of Taylor and McLennan (1995)

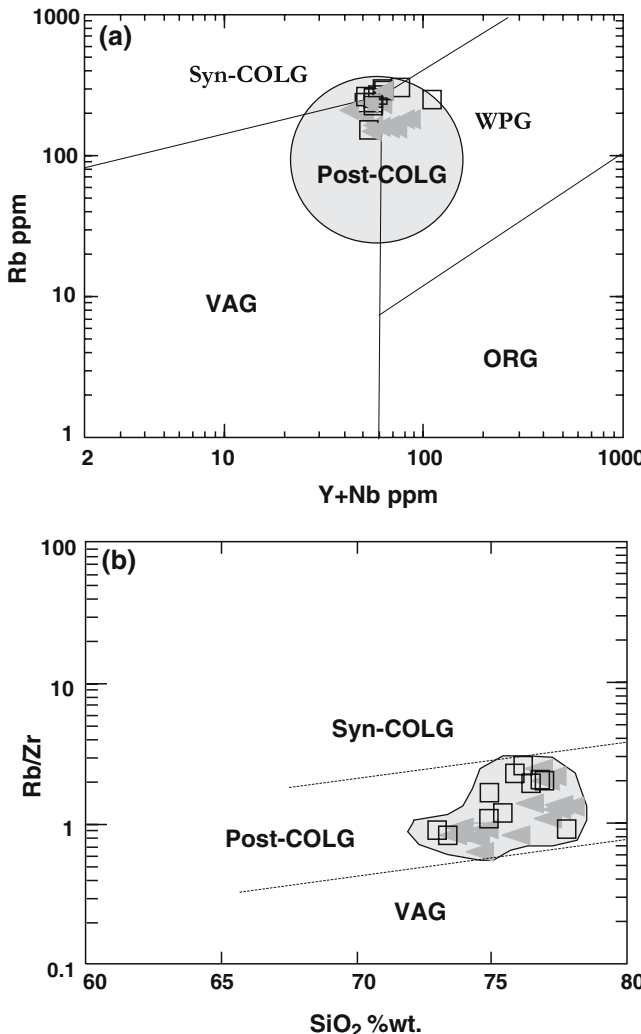


**Fig. 10** Tectonic discrimination diagrams of the felsic rocks of KCPS **a** after Pearce et al. (1984) and **b** after Harris et al. (1986)

enrichment in Th, U, La, Ce, Nd, Sm, Zr (Fig. 9a, b). However, the computed data in meta-rhyolites and meta-quartz porphyry rocks have slightly higher Ti and Sr values compared with the original rocks (Table 3). This may be due to the absence of mafic minerals and the secondary process.

For the REEs, the computed spider diagrams are also very similar to the KCPS rocks displaying enrichment in LREE, sharp Eu negative anomaly and low to unfractionated HREE, suggesting an optimal correlation by 18% fractional melting plus 18% Rayleigh fractional crystallization and 20% fractional melting plus 20% Rayleigh fractional crystallization of the upper continental crust rocks to produce both rock groups (Fig. 9c, d).

To summarize, petrogenetic modeling implies that both the meta-rhyolites and meta-quartz porphyries of KCPS were developed from an upper continental crustal source (partial melting of granites/felsic rocks) by 18–20% fractional melting plus 18–20 % Rayleigh fractional crystallization.

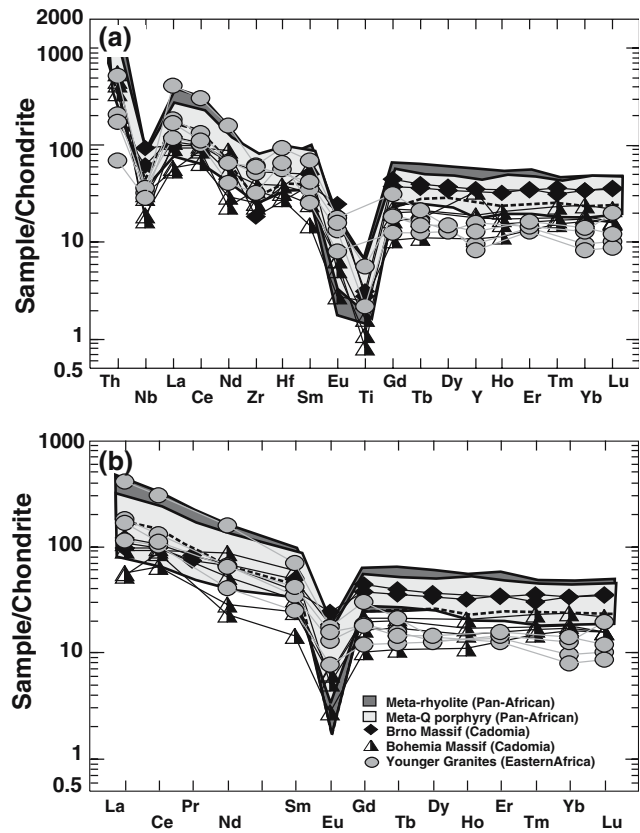


**Fig. 11** **a** Comparative chondrite-normalized multivariation and **b** REE diagrams (chondrite normalizing values are from Sun and McDonough 1989) and their correlation with some Late Pan-African granitoids as Eastern Africa, Bruno and Bohemian Massifs. Late Proterozoic felsic igneous rocks from northeast Africa (data from Rogers et al. 1978; Saleh 2001; El-Nisr et al. 2001), Bohemia (data from Dostal et al. 2001) and Bruno Massif (data from Finger et al. 2000)

## Tectonic setting

To interpret the tectonic setting of the felsic rocks of the KCPS the tectono-magmatic discrimination diagrams of Pearce et al. (1984) and Pearce (1996) were used. In the Rb versus Y + Nb tectonic discrimination diagram of Pearce et al. (1984), all KCPS rocks (meta-rhyolites and meta-quartz porphyry rocks) plot on the triple junction of within plate granites (WPG), syn-collision granites (syn-COLG), and volcanic arc granites (VAG) fields, which represents the field of post-collisional granites (post-COLG) of Pearce (1996) (Fig. 10a). On the Rb/Zr versus SiO<sub>2</sub> diagram of Harris et al. (1986), the felsic rocks of the KCPS plot within the post-collisional granites field (Fig. 10b) rather than in the syn-collision and volcanic arc granites field. Therefore it is suggested that the meta-rhyolites and the meta-quartz porphyry rocks of KCPS may have been emplaced during the post-orogenic period of crustal thinning (Genna et al. 2002) at the end of the Late Proterozoic.

## Comparison with Late Neoproterozoic granitoids

The average trace and REE patterns of the meta-rhyolites and meta-quartz porphyry rocks of the KCPS were correlated with the granitoids of Eastern Egypt (Arabian shield), Brno and Bohemia Massifs in Central Europe (Rogers et al. 1978; Saleh 2001; El-Nisr et al. 2001; Finger et al. 2000; Dostal et al. 2001) with Late Pan-African/Cadomian ages ranging from 550 to 530 Ma.

Chondrite-normalized trace element spider diagrams reveal that the KCPS rocks display very similar patterns with those from these North Gondwanan localities, where they have very similar sharp negative trends in Nb, Eu and Ti elements (Fig. 11a). The chondrite-normalized REE patterns of the KCPS samples and those from the Gondwana-derived areas also show concordant patterns with a clear enrichment of LREE compared with MREE and have a relatively unfractionated flat HREE (Fig. 11b).

## Discussion and conclusions

The Late Neoproterozoic meta-sedimentary host rocks of the granitoids in the Taurides, central Anatolia, are made up of dark gray phyllitic slates and/or phyllites with bands and lenses of black cherts (phthanite), cherty dolomites, dark gray meta-sandstones and debris flow conglomerates. The succession is very similar to those of the Gondwanan terranes in the Variscan Central and SW Europe (Brioverian sediments, e.g. Chantraine et al. 1988) as well as in NW Africa.

In the Taurides, the Late Proterozoic meta-sedimentary rocks are associated with dynamo-metamorphic rhyolites and are intruded by quartz porphyries. The latter yielded a single zircon evaporation minimum age of  $543 \pm 7$  Ma (Kröner and Sengör 1990), which is interpreted as the intrusion age. This age is confirmed by the  $^{207}\text{Pb}/^{206}\text{Pb}$  evaporation ages obtained from two populations with colorless, transparent, euhedral long-prismatic zircons from the meta-rhyolites (sample SG394 from the Merdiven Hill, see Fig. 1) that yielded a mean age of  $541.3 \pm 10.9$  Ma (M. Satır, 2004 written communication). These two age determinations firmly establish the Late Neoproterozoic intrusion age of the granitic magmatism in Taurides.

Geochemical features of this granitic magmatism are indicative of an upper crustal source and a co-genetic nature of both the intrusive and extrusive members. Geochemical modeling suggests that the KCPS rocks may have been produced by a two-stage process involving fractional melting and Rayleigh fractional crystallization from an upper crustal source (partial melting of granites/felsic rocks). In the first stage felsic magmas were derived from highly fractionated anatexic crustal melts and by the 18–20% degree of partial melting (fractional melting) which resulted in a highly felsic composition and were emplaced in an upper

crustal (shallow) magma chamber. By 18–20% Rayleigh fractional crystallization, this felsic magma produced the meta-rhyolites and meta-quartz porphyry rocks of the KCPS, respectively. REE data also indicate that the lower continental crust and upper mantle were not important in producing the co-genetic subalkaline felsic magmas of the KCPS.

Once the felsic magma is separated from the magma chamber it may have first produced the carapace of extrusive rocks (rhyolites and associated felsic tuffs within the Güvercinoluk Formation). Penecontemporaneously, the same felsic magma was emplaced as a dike complex to produce the intrusive rocks (quartz porphyry rocks) of KCPS.

Tectono-magmatic discrimination diagrams indicate that the felsic rocks of KCPS were formed in a post-collisional tectonic setting. This is in good agreement for the Late Pan-African geodynamic model proposed by Göncüoglu and Kozlu (2000). The model suggests that

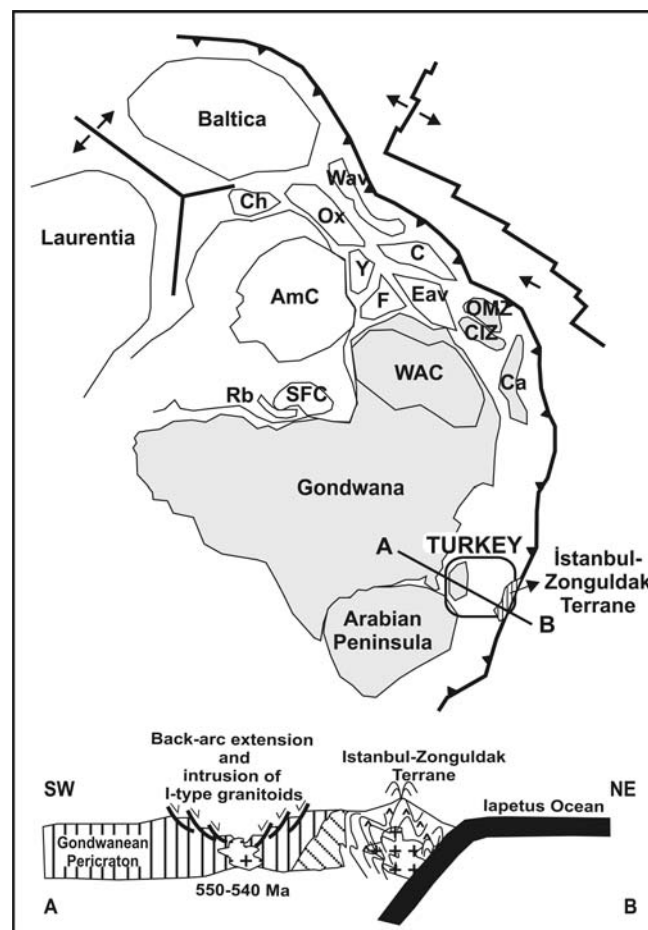


**Fig. 12** Schematic reconstruction of the Late Pan-African felsic rocks of KCPS (Turkey) during the Cadomian/Pan-African orogeny. AmC Amazonian craton, C Carolina, Ca Cadomia, Ch Chortis block, CIZ Central Iberian zone (Iberia), Eav East Avalonia, F Florida, OMZ Ossa-Morena zone (Iberia), Ox Oaxaquia, Rb Ribeira, SFC San Francisco craton, WAC West African craton, Wav West Avalonia, Y Yukatan, (modified after Nance et al. 2002; Murphy et al. 2002; Bandres et al. 2002)

felsic magmatism is the product of post-collisional extension within the northern margin of the Proterozoic Gondwana.

A geochemical comparison of the felsic igneous rocks of the KCPS in the Taurides with the Late Cadomian granitic magmatism in N Gondwana (e.g. Bandres et al. 2002; Murphy et al. 2002) suggests that they all display very similar petrological features and were probably formed by analogous geological processes and in similar tectonic settings (Fig. 12).

It is suggested that the Taurides were in a similar paleogeographic setting with the smaller Gondwana-derived terranes in North Africa and southern Europe (Spain, France, Iberia, Bohemia, Brno Massifs; e.g. Bandres et al. 2002) during the Late Proterozoic and Early Paleozoic. The geodynamic model presented in Fig. 12 suggests that during the Late Proterozoic (600–575 Ma) subduction was followed by the latest Proterozoic (575–550 Ma) diachronous arc-trench oblique collision along NW Gondwana. Between 550 and 540 Ma, the intrusion of mainly post-collisional I-type granitic rocks in the Taurides occurred. This may reflect the initial stages of rifting within the Gondwanan continental crust, accompanied by the mylonitic deformation within the granitoids and uplifting, as evidenced by the angular unconformity between the basement and by the overlying Early Cambrian fluvial deposits. The basal conglomerates contain deformed and dynamo-metamorphic pebbles of the basement rocks. This is a conclusive evidence for the relative age of the mylonitic basement-cover relations identified in Sandıklı area. Granitoid magmatism in the Taurides as well as the coeval ones in the peri-Gondwanan terranes in southern Europe are considered as products of the Cadomian event (Bandres et al. 2002; Genna et al. 2002; Murphy et al. 2002; Nance et al. 2002). The early-middle Cam-

brian (i.e. ca 540–520 Ma) siliciclastic-limestone platform development with typical back-arc-type basic volcanism (Gürsu and Göncüoglu 2005) are interpreted to reflect rifting by back-arc extension, where the Gondwanan peri-cratonic margin had been subject to the lithospheric thinning to produce the back-arc basin. This event also correlates with the development in Cadomia and the related peri-Gondwanan terranes (Finger et al. 2000). Post-collisional extension probably continued during the rest of the Early Paleozoic period and resulted in the separation of some micro-continents from Gondwana and hence was responsible for the initial opening of an ocean to the north of the Taurides (Fig. 12).

The model in Fig. 12 contradicts with the suggestion of Kröner and Sengör (1990) that the Taurides might have been part of the Angora craton and the Pan-African evolution in the Middle East may have been terminated by the collision of this micro-continent with the Gondwana during the Early Cambrian.

**Acknowledgments** This study was funded by the General Directorate of Mineral Research and Exploration (MTA) and State Planning Organization (MTA/DPT Project No. 16 AZ) and includes only limited data of the first author's PhD thesis. We would like to thank Prof. M. Satır for the single zircon analyses performed in the Tübingen University, Laboratory for Geochronology. The authors gratefully acknowledge the comments of Prof. B. Bonin and Prof. S.A. El-Nisr who reviewed a preliminary version of this paper. Constructive reviews by Prof. İbrahim Cemen and Prof. B. Clark Burchfield improved the manuscript and are very much appreciated.

## Appendix

Table a

**Table a** Parameters used in the modeling of fractional melting and Rayleigh fractional crystallization processes

Distribution Coefficients	Hornblende-melt	Biotite-melt	Quartz-melt	Plagioclase-melt	K-Feldspar-melt
Rb	0.014 <sup>a</sup>	3,200 <sup>b</sup>	0.041 <sup>b</sup>	0.105 <sup>b</sup>	1.750 <sup>b</sup>
Ba	0.044 <sup>a</sup>	6.360 <sup>c</sup>	0.022 <sup>b</sup>	0.310	6.120 <sup>a</sup>
Th		0.997 <sup>b</sup>	0.009 <sup>b</sup>	0.048 <sup>b</sup>	0.023 <sup>b</sup>
U		0.773 <sup>b</sup>	0.025 <sup>b</sup>	0.093 <sup>b</sup>	0.048 <sup>b</sup>
K	0.081 <sup>a</sup>	5.630	0.013 <sup>b</sup>	0.1	1.490
Nb	4,000 <sup>a</sup>	6,367 <sup>b</sup>		0.025	
La		5,713 <sup>b</sup>	0.015 <sup>b</sup>	0.380 <sup>b</sup>	0.080 <sup>b</sup>
Ce	1,520 <sup>a</sup>	4,357 <sup>b</sup>	0.014 <sup>b</sup>	0.267 <sup>b</sup>	0.037 <sup>b</sup>
Sr	0.022 <sup>a</sup>	0.120 <sup>3</sup>		4.400	3.870 <sup>a</sup>
Nd	4,260 <sup>a</sup>	2,560 <sup>b</sup>	0.016 <sup>b</sup>	0.203	0.035 <sup>b</sup>
Hf		0.703 <sup>b</sup>	0.030 <sup>b</sup>	0.148 <sup>b</sup>	0.033 <sup>b</sup>
Zr	4,000 <sup>a</sup>	1.197 <sup>b</sup>		0.135 <sup>b</sup>	0.030 <sup>b</sup>
Sm	7,770 <sup>a</sup>	2,117 <sup>b</sup>	0.014 <sup>b</sup>	0.165 <sup>b</sup>	0.025 <sup>b</sup>
Ti	7,000 <sup>a</sup>		0.038 <sup>b</sup>	0.05	
Tb		1.957 <sup>b</sup>	0.017 <sup>b</sup>		0.025 <sup>b</sup>
Y	6,000 <sup>a</sup>	1.233 <sup>b</sup>		0.130 <sup>b</sup>	
Yb	8,380 <sup>a</sup>	1.473 <sup>b</sup>	0.017 <sup>b</sup>	0.090 <sup>b</sup>	0.030 <sup>b</sup>
Eu	5,140 <sup>a</sup>	2.020 <sup>b</sup>	0.056 <sup>b</sup>	5.417 <sup>b</sup>	4.450 <sup>b</sup>
Lu	5,500 <sup>a</sup>	1.617 <sup>b</sup>	0.014 <sup>b</sup>	0.092 <sup>b</sup>	0.033 <sup>b</sup>
Er	12,000 <sup>a</sup>	0.350 <sup>a</sup>		0.045	
Gd	10,000 <sup>a</sup>	0.067		0.125 <sup>b</sup>	

Distribution coefficients are for intermediate silicic compositions

<sup>a</sup>Arth (1976), Y–Nb trace elements from Pearce and Norry (1979)

<sup>b</sup>Nash and Crearcraft (1985)

<sup>c</sup>Watson and Harrison (1983)

## References

- Arth JG (1976) Behaviour of trace elements during magmatic proses—a summary of theoretical models and their applications. *J Res U S Geol Survive* 4:41–47
- Ballèvre M, Le Goff E, Hébert R (2001) The tectonothermal evolution of the Cadomian belt of northern Brittany, France: a Proterozoic volcanic arc. *Tectonophysics* 331:19–43
- Bandres A, Eguiluz L, Gil Ibarguchi JJ, Palacios T (2002) Geodynamic evolution of a Cadomian arc region: the northern Ossa-Morena zone, Iberian massif. *Tectonophysics* 352:105–120
- Beard JS, Lofgren GE (1989) Effect of water on the composition of partial melts of greenstone and amphibolites at 1, 3 and 6.9 kb. *Sciences* 244:195–197
- Beard JS, Lofgren GE (1991) Dehydration melting and water-saturated melting of basaltic and andesitic greenstone and amphibolites at 1, 3, 6.9 kb. *J Petrol* 32:365–401
- Bozkaya Ö, Gürsu S, Göncüoglu MC (2004) Diagenetic to very low-grade metamorphic evolution of Precambrian-Mesozoic units in the Sandıklı area, Western Taurides, Turkey. In: Proceedings of 5th international symposium on eastern mediterranean geology, vol 1, pp 1098–1101
- Chantraine J, Chauvel JJ, Balé P, Denis E, Rabu D (1988) Le Briovérien (Protérozoïque supérieur à terminal) et l'orogenèse cadomienne en Bretagne (France). *Bull Soc Géol Fr* 5:815–829
- Chantraine J, Egal E, Thieblemont D, Le Goff E, Guerrot C, Ballèvre M, Guennoc P (2001) The Cadomian active margin (North Armorican Massif, France): a segment of the North Atlantic Pan-African belt. *Tectonophysics* 331:1–18
- Chappell BW, White AJR (1974) Two contrasting granite types. *Pac Geol* 8:173–174
- Collins WJ, Beams SD, White AJR, Chappell BW (1982) Nature and origin of A-type granites, with particular reference to south-eastern Australian. *Contrib Mineral Petrol* 80:189–200
- Condé CK (1993) Chemical composition and evolution of the upper continental crust: contrasting results from surface samples and shales. *Chem Geol* 104:1–37
- Dostal J, Patočka F, Pin C (2001) Middle/Late Cambrian intra-continental rifting in the Central West Sudetes, NE Bohemian Massif (Czech Republic): geochemistry and petrogenesis of the bimodal metavolcanic rocks. *Geol J* 36:1–17
- Dörr W, Zulauf G, Fiala J, Franke W, Vejnar Z (2002) Neoproterozoic to Early Cambrian history of an active plate margin in the Tepla-Barrandian unit—a correlation of U-Pb isotopic-dilution-TIMS ages (Bohemia, Czech Republic). *Tectonophysics* 352:65–85
- El-Nisr SA, El-Sayed MM, Saleh GM (2001) Geochemistry and petrogenesis of Pan-African late to post orogenic younger granitoids at Shalatin-Halaib, South Eastern Desert -Egypt. *J Afr Earth Sci* 33:261–282
- Erdogan B, Uchmann A, Güngör T, Özgül N (2004) Lithostratigraphy of the Lower Cambrian metaclastics and their age based on trace fossils in the Sandıklı region, southwestern Turkey. *Geobios* 38:346–360
- Finger F, Tichomirowa M, Pin C, Hanžl P (2000) Relics of an Early-Panafrican metabasite–metarhyolite formation in the Brno Massif, Moravia, Czech Republic. *Int J Earth Sci* 89:328–335
- Genna A, Nehlig P, Le Goff E, Guerrot C, Shanti M (2002) Proterozoic tectonism of the Arabian Shield. *Precambrian Res* 117:21–40
- Göncüoglu MC, Dirik K, Kozlu H (1997) General characteristics of pre-Alpine and Alpine Terranes in Turkey: explanatory notes to the terrane map of Turkey. *Ann Géologiques des Pays Hellénique* 37:515–536
- Göncüoglu MC, Kozlu H (2000) Early Paleozoic evolution of the NW Gondwanaland: data from southern Turkey and surrounding regions. *Gondwana Res* 3:315–323
- Gürsu S, Göncüoglu MC (2001) Characteristic features of the Late Precambrian felsic magmatism in Western Anatolia: implications for the Pan-African evolution in NW PeriGondvana. *Gondwana Res* 4(2):169–170
- Gürsu S (2002) Geology and petrogenesis of pre-Paleozoic magmatic rocks in the Inner Western Anatolia (SW Afyon) region. PhD Thesis, Hacettepe University, pp 1–204
- Gürsu S, Göncüoglu MC, Bayhan H (2004) Geology and geochemistry of the pre-Early Cambrian rocks in Sandıklı area: implications for the Pan-African evolution in NW Gondwanaland. *Gondwana Res* 7(4):923–935
- Gürsu S, Göncüoglu, MC (2005) Early Cambrian back-arc volcanism in the Western Taurides, Turkey: implications for the rifting along northern Gondwanan margin. *Geol Mag* 142(5) (in press)
- Helz RT (1976) Phase relations of basalts in their melting ranges at  $P_{H_2O} = 5$  kb. Part II. Melt composition. *J Petrol* 17:139–193
- Harris NBW, Pearce JA, Tindle AG (1986) Geochemical characteristics of collision zone magmatism. In: Coward MP, Reis AC (eds) Collision tectonics. Geological Society of London Special Publication, vol 19, pp 67–81
- Ketin İ (1966) Cambrian formations in southeast Anatolia and their correlation with the Cambrian of eastern Iran. *Miner Res Explor Bull* 66:75–87
- Kozlu H, Göncüoglu MC (1995) Infracambrian units in Sandıklı area. In: Göncüoglu MC, Derman AS (eds) Guide Book to Early Palaeozoic in NW Gondwana. Turkish Association Petroleum Geologists Special Publication vol 2, pp 11–13
- Kozlu H, Göncüoglu MC (1997) Stratigraphy of the Infracambrian rock-units in the Eastern Taurides and their correlation with similar units in Southern Turkey. In: Göncüoglu MC, Derman AS (eds) Early Palaeozoic in NW Gondwana. Turkish Association Petroleum Geologists Special Publication, vol 3, pp 50–61
- Kröner A, Sengör AMC (1990) Archean and Proterozoic ancestry in the Late Precambrian to Early Paleozoic crustal elements of southern Turkey as revealed by single zircon dating. *Geology* 18:1186–1190
- Le Corre C (1977) Le Briovérien de Bretagne Centrale: essai de synthèse lithologique et structurale. *Bull BRGM* 3:219–253
- Murphy JB, Eguiluz L, Zulauf G (2002) Cadomian Orogens, peri-Gondwanan correlatives and Laurentia–Baltica connections. *Tectonophysics* 352:1–9
- Mushkin A, Navon O, Halicz L, Hartmann G, Stein M (2003) The petrogenesis of A-type magmas, from the Amram Massif, Southern Israel. *J Petrol* 44:815–832
- Nash WP, Creecraft HR (1985) Partition coefficient for trace elements in silicic magmas. *Geochim Cosmochim Acta* 49:2309–2322
- Nance RD, Murphy JB, Keppie JD, O'Brien SJ (2002) A Cordilleran model for the evolution of Avalonia. *Tectonophysics* 352:11–31
- Öngür T (1973) Bati Toroslar, Isparta bükümü kuzey kenarı çevresinde jeolojik gelişme. In: Proceedings of geological congress for the 50th anniversary of the Turkish republic, vol 1, pp 95–102
- Özgül N, Bölkübası S, Alkan H, Öztas Y, Korucu M (1991) Tectonostratigraphic units of the Lake District, Western Taurides, Tectonics and hydrocarbon potential of Anatolia and surrounding regions. In: Turgut S (eds) O. Sungurlu symposium proceedings, vol 1, pp 213–237
- Pearce JA (1996) Sources and setting of granitic rocks. *Episodes* 19:120–125
- Pearce JA, Norry MJ (1979) Petrogenetic implications of Ti, Zr, Y and Nb variations in volcanic rocks. *Contrib Mineral Petrol* 69:33–47
- Pearce AJ, Harris WN, Tindle GA (1984) Trace element discrimination diagrams for the tectonic interpretation of granitic rocks. *J Geol* 25:956–983
- Pin C, Linán E, Pascual E, Donaire T, Valenzuela A (2002) Late Proterozoic crustal growth in the European Variscides: Nd isotope and geochemical evidence from the Sierra de Cordoba andesites (Ossa-Morena Zone, southern Spain). *Tectonophysics* 352:133–151
- Rogers JJW, Ghuma MA, Nagy RM, Greenberg JK, Fullagar PD (1978) Plutonism in Pan-African belts and the geological evolution of northeastern Africa. *Earth Planet Sci Lett* 39:109–117

- Rollinson H (1993) Using geochemical data: evaluation, presentation, interpretation. Wiley, New York, pp 1–352
- Saleh GH (2001) Evolution of Pan-African A- and I-type granites from the southeastern Egypt: inferences from geology, geochemistry and mineralization. *Int Geol Rev* 43: 548–564
- Spulber SD, Rutherford MJ (1983) The origin of rhyolite and plagiogranite in oceanic crust: an experimental study. *J Petrol* 24:1–25
- Sun SS, McDonough WF (1989) Chemical and isotopic systematics of oceanic basalts: implications for mantle composition and processes. In: Saunders AD, Norry MJ (eds) Magmatism in ocean basins. Geological Society of London Special Publication, vol 42, pp 313–345
- Taylor SR, McLennan SM (1995) The geochemical evolution of the continental crust. *Rev Geophys* 33:241–265
- Watson EB, Harrison MT (1983) Zircon saturation revisited: temperature and composition effects in a variety of crustal magma types. *Earth Planet Sci Lett* 64:295–304
- Winchester AJ, Floyd AP (1977) Geochemical discrimination of different magma series and their differentiation products using immobile elements. *Chem Geol* 20:325–343
- Winther KT, Newton RC (1991) Experimental melting of hydrous low-K tholeiite: evidence on the origin of Archean craton. *Bull Geol Soc Den* 39:213–228
- Wolf MB, Wyllie PJ (1994) Dehydration melting of amphibolites at 10 kbar: the effects of temperature and time. *Contrib Mineral Petrol* 115:369–383